Stable multipole solitons in defocusing saturable media with an annular trapping potential

XIAOLI LANG¹, BORIS A. MALOMED ² AND LIANGWEI DONG^{1,*}

Abstract: We systematically investigate the existence, stability, and propagation dynamics of multipole-mode (necklace-shaped) solitons in the two-dimensional model of an optical medium with the defocusing saturable nonlinearity and an annular potential trough. Various families of stable multipole solitons trapped in the trough, from dipole, quadrupole, and octupole ones to multi-lobe complexes, are found. The existence domain remains invariant with the increase of the potential's depth. Solitons with a large number N of lobes are stable in a wide parameter region, up to N = 48 and even farther. Actually, stable multipole solitons of an arbitrarily high order N can be found, provided that the trough's radius is big enough. The power of stable multipoles is essentially larger in comparison to previously studied models. It is demonstrated analytically and numerically that the application of a phase torque initiates stable rotation of the multipole complexes. Thus, we put forward an effective scheme for the stabilization of multipole solitons with an arbitrary high number of lobes, including rotating ones, which offers new possibilities for manipulating complex light beams.

© 2025 Optica Publishing Group

1. Introduction

The stabilization of high-power multipole solitons with a large number of poles (lobes) is a challenging problem in nonlinear optics [1, 2], quantum matter (especially Bose-Einstein condensates, BECs), and other physical settings [3]. The primary difficulty arises from the increasingly strong repulsive interaction between adjacent out-of-phase lobes, which must be balanced by a holding factor.

Multipole (alias "necklace-shaped" [4,5]) solitons are characterized by an even number N of lobes (alias "beads") uniformly distributed along a ring. The phase alternation between adjacent lobes prohibits the existence of odd-N configurations, with the exception of the fundamental one (N=1), which corresponds to the axisymmetric ground-state mode. The simplest structured state is the dipole soliton with N=2. While nonlinearity can partly counteract diffraction in the single-component multipole modes, their long-distance propagation in the free space is ultimately limited by either the radial expansion [4] or spiral instability [5].

Two-dimensional (2D) multipole solitons were first predicted in a two-component system exhibiting focusing saturable nonlinearity [6, 7], where a stable necklace-shaped configuration in one component is maintained by its interaction with a fundamental mode in the second component, mediated by the XPM (cross-phase-modulation) nonlinearity. On the other hand, the expansion of necklace beams in focusing Kerr (non-saturable) media can be slowed down by imprinting an angular momentum onto the pattern [8]. Suppression of the expansion of the necklace structures was also demonstrated in systems with fractional diffraction and saturable nonlinearities [9]. Metastable necklace beams have been predicted in systems with competing quadratic-cubic [10] and cubic-quintic (CQ) [11, 12] nonlinearities. Experimental observations of such patterns have been reported in local [13] and nonlocal [14] nonlinear media.

^{*}dlw 0@163.com

Department of Physics, Zhejiang University of Science and Technology, Hangzhou, 310023, China

² Instituto de Alta Investigacion, Universidad de Tarapaca, Casilla 7D, Arica, Chile

Photonic lattices (PhLs), induced by spatially-periodic transverse modulations of the local refractive index in optical media, provide a powerful tool for stabilizing various nonlinear states by means of the effective trapping potential [15–17]. In particular, multipole-mode solitons can be supported by diverse PhL and waveguiding structures [18–28]. In addition to multipole solitons supported by spatially periodic [19–22] and quasiperiodic [29] PhLs, stable nonlinear multipole-modes were demonstrated in \mathcal{PT} -symmetric lattices [24, 25], circular waveguiding arrays [28], and axially symmetric Bessel PhLs [26, 27, 30].

Beyond optics, multipole patterns with various values of *N* have been predicted in BECs featuring both contact [31] and dipole-dipole [32] interactions. In binary BEC systems, the analysis has predicted metastable quantum droplets arranged in ring-shaped cluster configurations [33]. The corresponding system is based on the Gross-Pitaevskii equations with the Lee-Huang-Yang corrections, that account for beyond-mean-field effects [34, 35]. In particular, stable multipole quantum droplets can be supported by weakly anharmonic trapping potentials [36].

While extensive efforts were put forth to suppress the instability of multipole solitons, arising from the repulsive interaction between adjacent lobes, the prediction of stable modes with large pole numbers N remains a significant challenge, especially for high-power states. Previous studies primarily addressed lower-order multipole solitons, particularly dipoles (N = 2) and quadrupoles (N = 4). Such stable modes exist in CQ nonlinear media, with a combination of the 2D harmonic-oscillator trap and a circular Gaussian potential barrier [37]. However, the respective solitons with $N \ge 8$ poles exhibit instability in their entire existence domain. Multipole modes with N = 16 can be made stable in CQ media with an annular potential, but the respective stability region is very narrow and the corresponding power is very low [38].

In this work, we propose a realistic setup that enables the self-trapping of stable solitons with large pole numbers. The combination of the defocusing saturable nonlinearity and an engineered ring-shaped potential maintains distinct families of multipole solitons, whose radius and radial thickness can be controlled by adjusting the radius and width of the confining annular potential. The respective stability domain shrinks $very\ slowly$ with the growth of N, permitting stable solitons, at least, up to N=26 for typical parameters of the potential. Furthermore, the power of stable multipole solitons is remarkably enhanced in comparison with the previous studies, which is crucially important for potential applications in photonics, where one would like to use bright beams. Thus, the most important conclusion is that one can produce stable multipole-mode states with an arbitrary high order (pole number), N, and arbitrarily high power, by selecting a sufficiently large radius of the potential trough. We also demonstrate robust rotation of the multipole solitons, driven by a phase torque.

The subsequent presentation is structured as follows. The model, based on the 2D Schrödinger equation with the self-defocusing saturable nonlinearity and annular-trough trapping potential, is introduced in Section 2. The results of the systematic analysis are reported in Section 3. The paper is concluded by Section 4.

2. The model

We consider the propagation of optical beams along the z-axis in the bulk medium with the saturable defocusing term and a transverse modulation of the refractive-index profile, which induces an effective axisymmetric trapping potential. The evolution of the optical-wave amplitude Ψ is governed by the 2D nonlinear Schrödinger (NLS) equation, written in the normalized form:

$$i\frac{\partial\Psi}{\partial z} = -\frac{1}{2} \left(\frac{\partial^2\Psi}{\partial x^2} + \frac{\partial^2\Psi}{\partial y^2} \right) + \frac{|\Psi|^2}{1 + s|\Psi|^2} \Psi - pV(r)\Psi, \tag{1}$$

where s quantifies the saturability of the nonlinear response. The transverse (x, y) and longitudinal z coordinates are scaled, severally, by the width and diffraction length of the input beam.

The trapping annular-trough potential, with $r \equiv \sqrt{x^2 + y^2}$, depth p > 0, ring radius r_0 , and width d, is

$$-pV(r) = -p \exp\left[-\frac{(r-r_0)^2}{d^2}\right].$$
 (2)

Equation (1) conserves the integral power,

$$U = \iint |\Psi(x, y)|^2 dx dy,$$
 (3)

along with the angular momentum,

$$M = i \iint \Psi^* \left(y \frac{\partial \Psi}{\partial x} - x \frac{\partial \Psi}{\partial y} \right) dx dy \tag{4}$$

(* stands for the complex conjugate), and Hamiltonian,

$$H = \iint \left\{ \frac{1}{2} |\nabla \Psi|^2 + \frac{1}{s} \left[|\Psi|^2 - \frac{1}{s} \ln \left(1 + s |\Psi|^2 \right) \right] - pV(r) |\Psi|^2 \right\} dx dy.$$
 (5)

Figure 1(a) shows the ring-shaped potential defined by Eq. (2), which is subject to constraint $V(r=r_0-r')=V(r=r_0+r')$ for all $0 < r' < r_0$. This feature plays a crucial role in the stabilization of the nonlinear modes, as it ensures identical waveguiding conditions in the inner $(r < r_0)$ and outer $(r > r_0)$ annular regions. Previous works have demonstrated that, in models with different nonlinearities, annular potential (2) supports three species of stable states: multipole modes [38], vortex solitons carrying the integer winding number (topological charge) [39], and higher-order vortex quantum droplets in binary BECs [40]. For small s, the saturable defocusing nonlinearity in Eq. (1) reduces to the cubic-quintic form with the defocusing cubic $(-|\Psi|^2\Psi)$ and focusing quintic $(+s|\Psi|^4\Psi)$ terms. This sign combination is fundamentally different from the model in Refs. [38,39], which used the focusing cubic $(+|\Psi|^2\Psi)$ and defocusing quintic $(-|\Psi|^4\Psi)$ terms. Note that the focusing quintic term $(+s|\Psi|^4\Psi)$ with small s can be neglected for typical soliton intensities, as its contribution remains small compared to the dominant cubic term.

We search for stationary solutions of Eq. (1) as per the usual ansatz,

$$\Psi(x, y, z) = \psi(x, y) \exp(ibz), \tag{6}$$

with real propagation constant b and the transverse field profile, $\psi(x, y)$. It satisfies the equation

$$\frac{1}{2} \left(\frac{\partial^2 \psi}{\partial x^2} + \frac{\partial^2 \psi}{\partial y^2} \right) - b\psi + pV(r)\psi - \frac{|\psi|^2}{1 + s|\psi|^2} \psi = 0, \tag{7}$$

which can be solved by means of iterative methods, viz., either the relaxation algorithm or Newton-conjugate-gradient one [2]. The solutions form continuous families parameterized by propagation constant b, saturation parameter s, potential depth p, and coefficients r_0 and d of potential (2).

The linear-stability analysis of the stationary solutions can be performed by adding small perturbations, with real and imaginary components, u(x, y) and v(x, y), and complex eigenvalue λ , to the stationary solution, so that the perturbed solution is

$$\Psi(x, y, z) = \{\psi(x, y) + [u(x, y) + iv(x, y)] \exp(\lambda z)\} \exp(ibz). \tag{8}$$

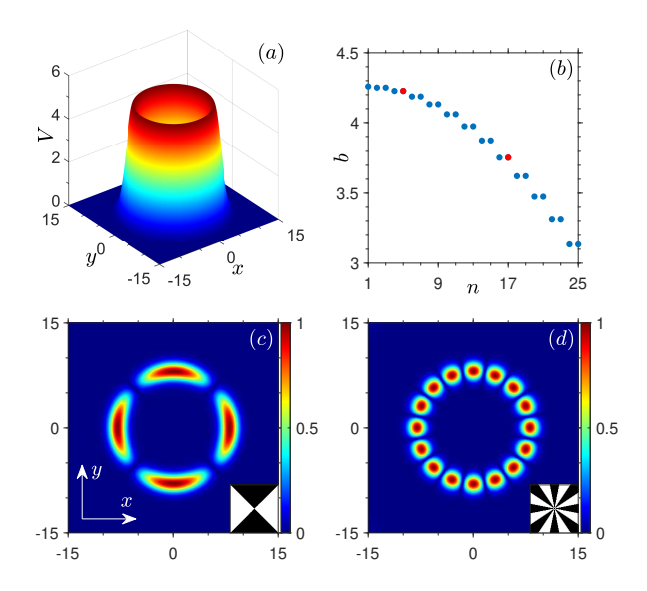


Fig. 1. (a) The annular potential, as defined by Eq. (2) (it is plotted here with factor p). (b) A typical spectrum of discrete eigenvalues b of the linearized version of equation (7) with this potential. Values of n denote the number of the eigenmode. (c, d) Absolute values of the wave function, $|\psi(x, y)|$, in the quadrupole and 16-pole linear eigenstates with eigenvalues marked by two red dots in (b). The insets display the corresponding phase structures. The parameters of the annular potential are $r_0 = 8$, d = 2, and p = 5.

The substitution of this in Eq. (1) and linearization with respect to the perturbation yields the eigenvalue problem,

$$\lambda u = -\frac{1}{2} \left(\frac{\partial^2}{\partial x^2} + \frac{\partial^2}{\partial y^2} \right) v + bv - pVv + \frac{\psi^2 + s\psi^4}{(1 + s\psi^2)^2} v$$

$$\lambda v = \frac{1}{2} \left(\frac{\partial^2}{\partial x^2} + \frac{\partial^2}{\partial y^2} \right) u - bu + pVu - \frac{3\psi^2 + s\psi^4}{(1 + s\psi^2)^2} u,$$
(9)

that can be solved numerically by means of the Fourier collocation algorithm [2]. The underlying soliton is stable if the solution of Eq. (9) yields only imaginary eigenvalues, the instability growth rate (if any) being $Re(\lambda)$.

Prior to producing multipole modes in the framework of the full nonlinear equation (1), it is instructive to analyze the spectrum of its linearized counterpart with the same potential (2), as nonlinear modes usually bifurcate from linear eigenstates. The numerically computed spectrum of the linearized equation comprises a finite set of discrete real eigenvalues, as shown in Fig. 1(b), along with the obvious continuous spectrum (not shown here). Note that linear modes with more poles corresponding to the eigenvalues with n > 25 still exist. Increasing the potential depth p induces a rightward shift in the eigenvalue spectrum, the variation of the thickness d and radius r_0 also affecting the eigenvalue distribution. The number of guided modes increases with the radius r_0 . In the limit of $r_0 \to \infty$, the system reduces to the 2D equation with a quasi-1D trapping potential, V(x). While V(x) itself supports only a finite number of trapped transverse modes, the inclusion of a longitudinal plane-wave factor $\exp(iky)$ allows for the construction of infinitely many guided modes, parameterized by the wavenumber k.

The spectrum reveals an essential symmetry property: while the ground-state eigenvalue remains nondegenerate, in agreement with the fundamental principle of quantum mechanics [41],

all excited states exhibit double degeneracy, with mutually orthogonal eigenmodes sharing identical eigenvalues. The degeneracy implies that the linear eigenmodes with $N \ge 2$ poles correspond, specifically, to the N-th and N+1-th eigenvalues. Representative examples of these eigenmodes are displayed in Figs. 1(c) and (d) for the fourth and sixteenth excited states, respectively. The linear system permits arbitrary superpositions of the mutually degenerate eigenmodes as valid solutions. A notable example occurs for the dipole modes (N=2), where superpositions of the orthogonal states generate two vortex solutions with topological charges $m=\pm 1$, demonstrating the direct relationship between the multipole states and those carrying the angular momentum.

3. Results and discussion

3.1. Dipole and quadrupole solitons

We now address multipole-mode solitons in the defocusing saturable nonlinear medium. The dipole modes consist of two arc-shaped fragments with the π -phase difference between them, localized on the ring of radius r_0 , as shown in Figs. 2(b, c). Both the peak amplitude and thickness of the dipole solitons monotonously increase with the decrease of the propagation constant b. Quadrupole solitons exhibit a more complex structure, composed of four fragments, with the π -phase shift between adjacent ones, see Figs. 2(d, e). For the same potential, the angular span of individual arc-shaped fragments in the quadrupoles is naturally smaller than in their dipole counterparts.

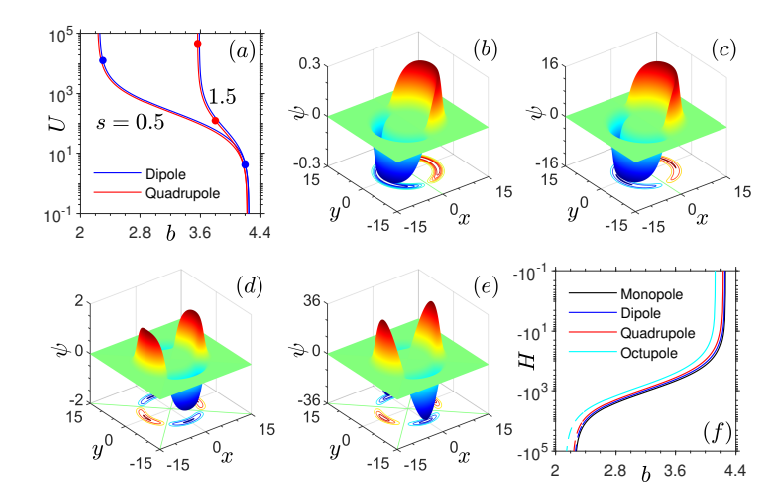


Fig. 2. (a) Integral power (3) versus propagation constant b for dipole and quadrupole solitons in the annular potential (2) with the saturation parameters s=0.5 and 1.5. (b, c) Examples of stable low-power (b=4.2) and unstable high-power (b=2.3) dipole modes marked by blue dots in (a). (d, e) Examples of stable moderate-power (b=3.8) and unstable high-power (b=3.563) quadrupoles marked by red dots in (a). (f) The Hamiltonian of multipole modes versus b. Solid and dashed lines denote the stable and unstable segments. The parameters are $r_0=8$, d=2 and p=5. s=0.5 in (b, c) and 1.5 in (d, e).

In Fig. 2(a), the soliton families, built according to definition (6), stem from the corresponding linear eigenmodes, at upper-cutoff values of the propagation constant, $b_{\rm upp} = 4.251$ for the dipoles and $b_{\rm upp} = 4.227$ for quadrupoles, which precisely coincide with the respective linear eigenvalues shown in Fig. 1(b) (obviously, these values do not depend on the saturation constant s). At s = 0.5, the power diverges at the lower cutoff, $b_{\rm low} = 2.251$ for the dipoles and

 $b_{\text{low}} = 2.227$ for the quadrupoles. As illustrated below by Fig. 3(d), the divergence of the integral power is related to diverging values of the local power, $|\Psi|^2$, for which the nonlinear saturable term in Eq. (1) is asymptotically replaced by the linear one, $s^{-1}\Psi$, hence the cutoff values of the propagation constant are obviously related:

$$b_{\rm upp} = b_{\rm low} + 1/s,\tag{10}$$

which is indeed corroborated by the numerical results [see, e.g., the curves for s = 0.5 and 1.5 in Fig. 2(a)]. This relation is known for soliton families in other models with saturable nonlinearity, including 1D soliton trains in harmonic PhLs [42] and 2D broken-ring solitons in Bessel lattices [43].

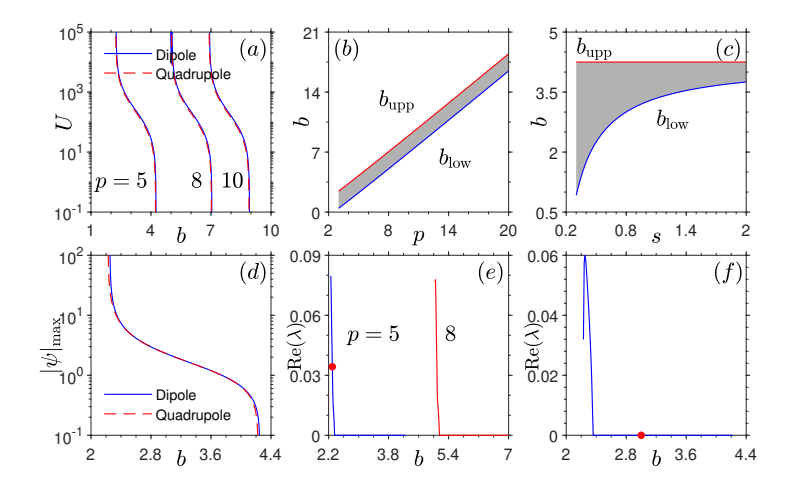


Fig. 3. (a) Power U vs. propagation constant b for dipole and quadrupole solitons, for s=0.5 and varying values of p. (b) The existence domain of the dipole solitons for s=0.5 and varying p, which agrees with relation (10). (c) The existence domain of the dipole solitons for p=5 and varying values of s. (d) The peak value $|\psi|_{\text{max}}$ of the dipole and quadrupole solitons vs. b at s=0.5, p=5. (e) The instability growth rate $\text{Re}(\lambda)$ vs. b for the dipole solitons at s=0.5. (f) The same for the quadrupole solitons at s=0.5, p=5. Other parameters are s=0.5, s=0.5,

As the potential depth p increases, the existence domain undergoes a systematic rightward shift, see Figs. 3(a, b), while the shape of the U(b) dependence remains approximately invariant. This feature is naturally explained by the fact that the eigenvalue of each bound state in a deep potential well stays at approximately constant distance from the well's bottom. Further, relation (10) explains the rapid contraction of the existence domain for the dipole and quadrupole solitons with the increase of the saturation constant s, see Fig. 3(c).

As seen in Fig. 2(a), the power of the solitons with different values of N (in that figure, these are N=2 and 4), is a monotonously decreasing function of propagation constant b, hence the families satisfy the *anti-Vakhitov-Kolokolov* (anti-VK) criterion, dU/db < 0, which is a necessary stability condition for solitons supported by a defocusing nonlinearity [44] (the VK criterion per se is opposite, dU/db > 0, applying to models with focusing nonlinearity [45,46]). A comprehensive linear-stability analysis of the dipole and quadrupole soliton families has been performed on the basis of the numerical solution of the eigenvalue problem (9), with representative results plotted in Figs. 3(e) and (f). For the dipole solitons in the potential with p=5, the stable-propagation regime spans $b \in [2.35, 4.25]$, covering approximately 95% of the total existence domain, $b \in [2.25, 4.25]$. When the potential depth increases to p=8, the stability region shifts to $b \in [5.14, 7.04]$ while maintaining the same relative extent

(95%) of the respective existence domain, $b \in [5.04, 7.04]$ [see Fig. 3(e)]. Thus, the relative width of the stability region remains approximately invariant with the increase of the potential depth. Quadrupole solitons exhibit similar stability characteristics, with a stability range of $b \in [2.36, 4.22]$, that encompasses about 93% of their existence domain, $b \in [2.22, 4.22]$ [see Fig. 3(f)].

3.2. Multipole solitons

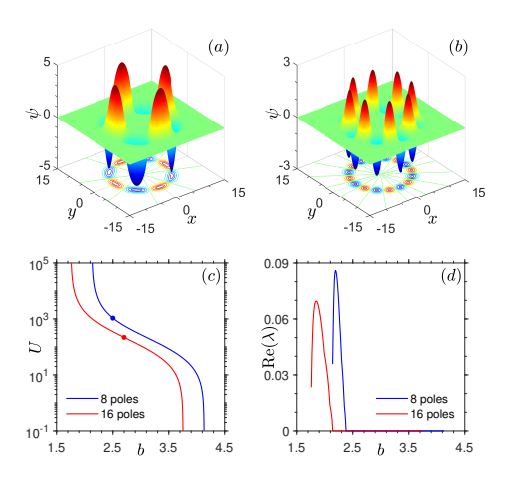


Fig. 4. (a,b) The shapes of 8-pole soliton at b=2.5 and 16-pole soliton at b=2.7. The corresponding points are marked by dots in panel (c), which displays integral power U vs. propagation constant b for the 8- and 16-pole solitons. (d) The instability growth rate $\text{Re}(\lambda)$ vs. b for the 8-pole and 16-pole solitons. The parameters are $r_0=8$, d=2, s=0.5, and p=5.

Next, we consider multipole solitons of a higher order N. Figures 4(a) and (b), respectively, display the stationary field distributions in the 8-pole and 16-pole solitons confined within the annular potential trough. Regardless of N, all multipole solitons keep the alternating-sign phase structure between neighboring lobes. Compared to the dipole and quadrupole modes displayed above in Figs. 2(b-d), these higher-order solitons naturally exhibit tighter packaging of adjacent fragments. As expected, relation (10) holds for them too, see Fig. 4(c). The large difference between the integral powers of the 8- and 16-pole solitons, in comparison to the smaller difference between the dipoles and quadrupoles [see Fig. 2(a) above] originates from the large separation between the corresponding eigenvalues of the linear spectrum, as is made evident by Fig. 1(b).

The key finding of this work is that multipole-mode solitons maintain remarkably broad stability domains across in the underlying parameter space, even for high pole numbers N. In particular, the stability regions of the 8- and 16-pole solitons cover, respectively, 88% and 80% of their existence domains, as seen in Fig. 4(d), in drastic contrast to multipole solitons in the CQ model with the same potential, where the instability occupies a dominant share of the existence domain [38]. The stability properties reported here are particularly significant for two reasons: (i) the stability regions for multipole-mode solitons expand steeply; and (ii) there exist stable high-power multipole solitons, that were previously unattainable.

To further elucidate properties of the multipole solitons of extremely high orders, we display an example of a 26-lobe one in Figs. 5(a, b). The potential squeezes the lobes along the angular direction, leading to extremely tight packaging and the strong repulsive interaction between adjacent lobes. Ultimately, it overcomes the trapping capability of the annular potential trough. Therefore, the 26-pole solitons are unstable in their nearly entire existence domain, see Fig. 5(c).

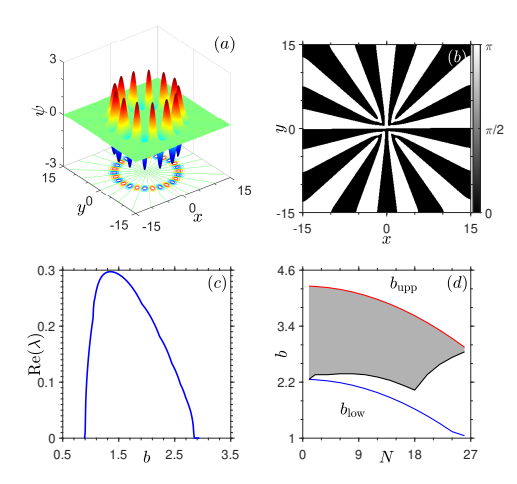


Fig. 5. (a, b) The field and phase shapes of the 26-pole soliton at b=2. (c) The instability growth rate $\text{Re}(\lambda)$ vs. b for the family of 26-pole solitons. (d) The existence area (between the b_{low} and b_{upp} curves) and the stability region (shaded) vs. the pole number N. The parameters are $r_0=8$, d=2, s=0.5, and p=5.

Nevertheless, the stability is definitely maintained for the multipoles with $N \le 18$ in a substantial part of their parameter space, as shown in Fig. 5(d). At N > 18, the stability region quickly shrinks, implying a fundamental limit for the stability of the higher-order multipole solitons.

As said above, the primary mechanism of the instability of the multipole solitons with a large number N of the lobes originates from the repulsion between adjacent ones, generating a net outward force that tends to destroy the necklace structure of the circular soliton chain. To counteract this effect, one can increase radius r_0 of the annular potential trough (2), aiming to reduce the strength of the inter-lobe repulsion, thereby enabling the generation of stable multipole solitons with still large N. To corroborate this possibility, in Fig. 6 we present examples of stable quadrupole and 48-pole solitons, which are trapped in the potential with a large radius. In this case, two effects are observed: (i) following the increase of the integral power, the arc-shaped segments elongate [Figs. 6(a, b)]; (ii) individual lobes in the necklace-like solitons exhibit nearly circular profiles, see Fig. 6(c). Remarkably, in Fig. 6(d), the 48-pole solitons remain stable across 79% of their existence domain, thus representing the highest pole number reported to date for stable multipole solitons. In principle, stable multipole solitons with arbitrarily high N can be created through the appropriate scaling of the potential-trough radius.

To verify the predictions of linear-stability analysis, we have conducted comprehensive numerical simulations of the perturbed soliton propagation, using the split-step Fourier method. For the stability test, we added white-noise perturbations to the input at z = 0. Representative examples of the evolution are produced in Fig. 7. At b = 2.3, the dipole soliton is deformed at z = 660 [Fig. 7(a)], which is consistent with its finite but small instability growth rate [Re(λ) = 0.034, see Fig. 3(e)]. The nonzero instability growth rates are complex, indicating the presence of an oscillatory instability. This instability eventually results in oscillations of the two arc-shaped segments on the ring: while one segment shrinks, the other one expands along the ring, swapping their roles in the next cycle of the evolution, see Visualization 1 for the propagation details. In contrast, the quadrupole and 24-pole solitons with Re(λ) = 0 maintain their initial profiles as long as the simulations were running, as shown in Figs. 7(b, c). The results of the simulation are in full agreement with the predictions of the linear-stability analysis for all the considered cases, including the solitons with high pole numbers N. For instance, the 48-pole soliton remains stable at z = 2000 [Fig. 7(d)], maintaining its stationary shape intact,

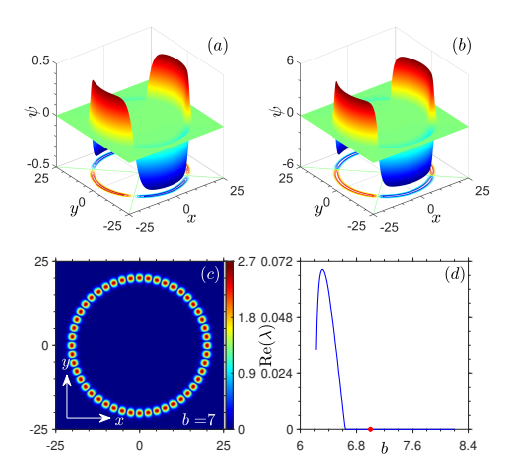


Fig. 6. Additional examples of stable multipole solitons trapped in the annular potential trough (2) with $r_0=20$. (a, b) Low-power and high-power quadrupole solitons at b=8.8 and 7.2, respectively. (c) The shape of $|\psi(x,y)|$ in the 48-pole soliton at b=7 marked by the red dot in panel (d), which displays the instability growth rate $\text{Re}(\lambda)$ vs. b for the 48-pole solitons. The parameters are $r_0=20$, d=2, s=0.5, and p=10.

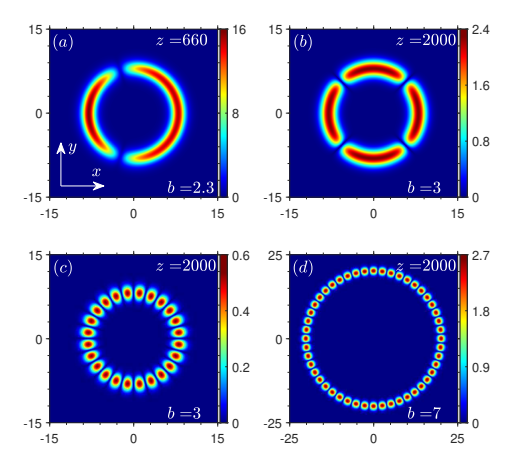


Fig. 7. The outcome of the unstable (a) (also see Visualization 1 for the process) and stable (b-d) perturbed propagation of the multipole solitons. The inputs used in (a) and (b) are marked by red dots in Fig. 3(e) and 3(f), respectively. (c) The outcome of the stable perturbed propagation of the 24-pole soliton. In panels (a-c) the parameters are $r_0 = 8$, d = 2, s = 0.5 and p = 5. (d) The outcome of the stable perturbed propagation of the 48-pole soliton marked by the red dot in Fig. 6(d), with parameters $r_0 = 20$, d = 2, s = 0.5 and p = 10.

cf. Fig. 6(c). The conclusion is that the perturbed stable solitons quickly shed off the initially added noise and maintain their structure in the course of indefinitely long evolution. Note that stable solitons with pole numbers $N \ge 20$ have rarely been found in previously studied models.

3.3. Rotating multipoles

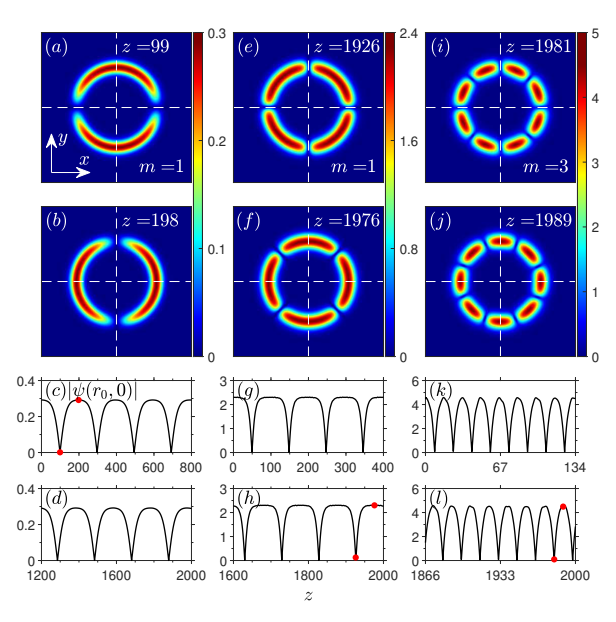


Fig. 8. The stable counter-clockwise rotation of the dipole with b=4.2 (a-d), quadrupole with b=3 (e-h), and 8-pole soliton with b=2.5 (i-l), initiated by the torque kick (11), with m=1 for dipole and quadrupole, and m=3 for the 8-pole. The initial profiles of the dipole amd 8-pole were taken as in Figs. 2(b) and 4(a), respectively. The bottom panels display the evolution of $|\Psi(x,y)|$ at the reference point, $(x,y)=(r_0,0)$, in indicated intervals of the propagation distance z. The configurations displayed in panels (a, b), (e, f) and (i, j) correspond to red dots in (c), (h) and (l), respectively. The parameters are $r_0=8$, d=2, s=0.5, and p=5.

The well-defined azimuthal structure of the multipole modes considered above makes it possible to set them in rotation by the application of a phase torque:

$$\psi(x, y) \to \psi(x, y) \exp(im\theta),$$
 (11)

where θ is the angular coordinate, and m is an integer topological charge (winding number). The resulting angular velocity of the rotating structure can be estimated as $\Omega \approx |m|/r_0^2$ [38], the corresponding rotation period being $Z_{\rm est} = 2\pi/\Omega \approx 2\pi r_0^2/|m|$. Numerical simulations confirm this expectation. In particular, the dipole soliton with $r_0 = 8$, kicked by the torque with m = 1, exhibits persistent rotation with period $Z_{\rm rot} \approx 396$ in Figs. 8(a, b), well matching the expected value, $Z_{\rm est} \approx 402$. Further, the simulations for the quadrupole soliton with the same parameters, $r_0 = 8$ and m = 1, produce the period $Z_{\rm rot} \approx 400$ in Figs. 8(e, f), which is also very close to $Z_{\rm est}$. Similarly, the 8-pole soliton with $r_0 = 8$ and m = 3 features $Z_{\rm rot} \approx 128$ in Figs. 8(i, j), while the respective estimate is $Z_{\rm est} \approx 134$. The rotation observed here, while somewhat similar to the rotating solitons trapped in a multiring potential [47], has a fundamentally different origin. In contrast to the whispering-gallery-like modes of [47], which are driven by a rotating potential, the multipole rotation here is initiated by the initial torque.

To demonstrate the robustness of the rotating multipoles, we track the evolution of the respective solution for $|\Psi(x, y)|$ at a reference point, $(x, y) = (r_0, 0)$. Bottom panels in Fig. 8

represent 5 full periods of the rotation of the dipole and quadrupole solitons, initiated by m = 1 in Eq. (11), and 15.6 periods for the 8-pole soliton, initiated by m = 3. In the course of the long propagation, the soliton profiles fully maintain their structural integrity. The stability of the rotating multispot patterns suggests their potential application to routing data-carrying optical beams, cf. Ref. [26].

4. Conclusion

In summary, we have systematically explored the existence conditions, stability, and propagation dynamics of 2D localized even-numbered multipole (necklace-shaped) configurations, in the framework of the NLS equation with the defocusing saturable nonlinearity and annular potential trough, in which the circular configurations are trapped. The multipoles are composed of alternating-phase lobes uniformly distributed along the trough. The stability domains of the multipole solitons in the parameter space shrink *very slowly* with the growth of the pole number N, permitting stable solitons, at least, up to N=48, which is a significant advancement beyond previously reported stability limits for N in other models. In comparison to the previous studies, the power of the stable multipole solitons is much larger, which is crucially important for potential applications to photonics. Thus, one can produce *stable* nonlinear multipole states, with an arbitrary large number of poles and arbitrarily high power, using the annular trapping potential with a sufficiently large radius. The robust rotational dynamics of the multipole solitons, induced by the application of the phase torque to them, has been demonstrated too.

Funding. National Natural Science Foundation of China (NSFC) (Grant No. 62575264).

Disclosures. The authors declare no conflicts of interest.

Data availability. Data underlying the results presented in this paper are not publicly available at this time but may be obtained from the authors upon reasonable request.

References

- 1. Y. S. Kivshar and G. P. Agrawal, Optical solitons: from fibers to photonic crystals (Academic press, 2003).
- 2. J. Yang, Nonlinear waves in integrable and nonintegrable systems (SIAM, 2010).
- 3. B. A. Malomed, Multidimensional Solitons (AIP Publishing LLC, 2022).
- M. Soljačić, S. Sears, and M. Segev, "Self-trapping of "necklace beams" in self-focusing Kerr media," Phys. Rev. Lett. 81, 4851 (1998).
- M. Soljačić and M. Segev, "Self-trapping of "necklace-ring" beams in self-focusing Kerr media," Phys. Rev. E 62, 2810 (2000).
- A. S. Desyatnikov, D. Neshev, E. A. Ostrovskaya, Y. S. Kivshar, W. Krolikowski, B. Luther-Davies, J. J. García-Ripoll, and V. M. Pérez-García, "Multipole spatial vector solitons," Opt. Lett. 26, 435–437 (2001).
- A. S. Desyatnikov, D. Neshev, E. A. Ostrovskaya, Y. S. Kivshar, G. McCarthy, W. Krolikowski, and B. Luther-Davies, "Multipole composite spatial solitons: theory and experiment," J. Opt. Soc. Am. B 19, 586–595 (2002).
- M. Soljačić and M. Segev, "Integer and fractional angular momentum borne on self-trapped necklace-ring beams," Phys. Rev. Lett. 86, 420 (2001).
- L. Dong, D. Liu, W. Qi, L. Wang, H. Zhou, P. Peng, and C. Huang, "Necklace beams carrying fractional angular momentum in fractional systems with a saturable nonlinearity," Commun. Nonlinear Sci. Numer. Simul. 99, 105840 (2021).
- Y. V. Kartashov, L.-C. Crasovan, D. Mihalache, and L. Torner, "Robust propagation of two-color soliton clusters supported by competing nonlinearities," Phys. Rev. Lett. 89, 273902 (2002).
- D. Mihalache, D. Mazilu, L.-C. Crasovan, B. A. Malomed, F. Lederer, and L. Torner, "Robust soliton clusters in media with competing cubic and quintic nonlinearities," Phys. Rev. E 68, 046612 (2003).
- D. Mihalache, D. Mazilu, L. C. Crasovan, B. A. Malomed, F. Lederer, and L. Torner, "Soliton clusters in threedimensional media with competing cubic and quintic nonlinearities," J. Opt. B 6, S333 (2004).
- T. D. Grow, A. A. Ishaaya, L. T. Vuong, and A. L. Gaeta, "Collapse and stability of necklace beams in Kerr media," Phys. Rev. Lett. 99, 133902 (2007).
- C. Rotschild, M. Segev, Z. Xu, Y. V. Kartashov, L. Torner, and O. Cohen, "Two-dimensional multipole solitons in nonlocal nonlinear media," Opt. Lett. 31, 3312–3314 (2006).
- J. Yang, I. Makasyuk, A. Bezryadina, and Z. Chen, "Dipole and quadrupole solitons in optically induced twodimensional photonic lattices: theory and experiment," Stud. Appl. Math. 113, 389

 –412 (2004).

- Y. V. Kartashov, B. A. Malomed, and L. Torner, "Solitons in nonlinear lattices," Rev. Mod. Phys. 83, 247–305 (2011).
- D. E. Pelinovsky, Localization in periodic potentials: from Schrödinger operators to the Gross-Pitaevskii equation, (Cambridge University, 2011).
- 18. Y. V. Kartashov and L. Torner, "Multipole-mode surface solitons," Opt. Lett. 31, 2172-2174 (2006).
- J. Yang, I. Makasyuk, A. Bezryadina, and Z. Chen, "Dipole solitons in optically induced two-dimensional photonic lattices," Opt. Lett. 29, 1662–1664 (2004).
- J. Yang, I. Makasyuk, P. G. Kevrekidis, H. Martin, B. A. Malomed, D. J. Frantzeskakis, and Z. Chen, "Necklacelike solitons in optically induced photonic lattices," Phys. Rev. Lett. 94, 113902 (2005).
- P. Rose, T. Richter, B. Terhalle, J. Imbrock, F. Kaiser, and C. Denz, "Discrete and dipole-mode gap solitons in higher-order nonlinear photonic lattices," Appl. Phys. B 89, 521–526 (2007).
- H. Susanto, K. J. H. Law, P. G. Kevrekidis, L. Tang, C. Lou, X. Wang, and Z. Chen, "Dipole and quadrupole solitons in optically-induced two-dimensional defocusing photonic lattices," Phys. D 237, 3123–3134 (2008).
- S. Xia, D. Song, L. Tang, C. Lou, and Y. Li, "Self-trapping and oscillation of quadruple beams in high band gap of 2D photonic lattices," Chin. Opt. Lett. 11, 090801 (2013).
- H. Wang, S. Shi, X. Ren, X. Zhu, B. A. Malomed, D. Mihalache, and Y. He, "Two-dimensional solitons in triangular photonic lattices with parity-time symmetry," Opt. Commun. 335, 146–152 (2015).
- H. Wang, X. Ren, J. Huang, and Y. Weng, "Evolution of vortex and quadrupole solitons in the complex potentials with saturable nonlinearity," J. Opt. 20, 125504 (2018).
- Y. V. Kartashov, R. Carretero-González, B. A. Malomed, V. A. Vysloukh, and L. Torner, "Multipole-mode solitons in Bessel optical lattices," Opt. Express 13, 10703–10710 (2005).
- 27. W.-P. Hong, "Surface multipole solitons on photorefractive media with Bessel optical lattices," J. Korean Phys. Soc. 66, 919–923 (2015).
- Y. V. Kartashov, B. A. Malomed, V. A. Vysloukh, and L. Torner, "Stabilization of multibeam necklace solitons in circular arrays with spatially modulated nonlinearity," Phys. Rev. A 80, 053816 (2009).
- 29. H. Sakaguchi and B. A. Malomed, "Gap solitons in quasiperiodic optical lattices," Phys. Rev. E 74, 026601 (2006).
- 30. L. Dong, J. Wang, H. Wang, and G. Yin, "Bessel lattice solitons in competing cubic-quintic nonlinear media," Phys. Rev. A 79, 013807 (2009).
- 31. B. B. Baizakov, B. A. Malomed, and M. Salerno, "Matter-wave solitons in radially periodic potentials," Phys. Rev. E 74, 066615 (2006).
- C. Huang, Y. Ye, S. Liu, H. He, W. Pang, B. A. Malomed, and Y. Li, "Excited states of two-dimensional solitons supported by spin-orbit coupling and field-induced dipole-dipole repulsion," Phys. Rev. A 97, 013636 (2018).
- Y. V. Kartashov, B. A. Malomed, and L. Torner, "Metastability of quantum droplet clusters," Phys. Rev. Lett. 122, 193902 (2019).
- D. S. Petrov, "Quantum mechanical stabilization of a collapsing Bose-Bose mixture," Phys. Rev. Lett. 115, 155302 (2015).
- 35. D. S. Petrov and G. E. Astrakharchik, "Ultradilute low-dimensional liquids," Phys. Rev. Lett. 117, 100401 (2016).
- L. Dong, D. Liu, Z. Du, K. Shi, and W. Qi, "Bistable multipole quantum droplets in binary Bose-Einstein condensates," Phys. Rev. A 105, 033321 (2022).
- 37. D. Liu, Y. Gao, D. Fan, and L. Zhang, "Multi-stable multipole solitons in competing nonlinearity media," Chaos Soliton. Fract. 173, 113691 (2023).
- 38. L. Dong, M. Fan, C. Huang, and B. A. Malomed, "Multipole solitons in competing nonlinear media with an annular potential," Phys. Rev. A 108, 063501 (2023).
- 39. L. Dong, M. Fan, and B. A. Malomed, "Stable higher-charge vortex solitons in the cubic-quintic medium with a ring potential," Opt. Lett. 48, 4817–4820 (2023).
- L. Dong, M. Fan, and B. A. Malomed, "Stable higher-order vortex quantum droplets in an annular potential," Chaos Soliton. Fract. 179, 114472 (2024).
- 41. L. D. Landau and E. M. Lifshitz, Quantum mechanics: non-relativistic theory, vol. 3 (Elsevier, 2013).
- 42. Y. V. Kartashov, V. A. Vysloukh, and L. Torner, "Soliton trains in photonic lattices," Opt. Express 12, 2831–2837 (2004).
- 43. L. Dong, J. Wang, H. Wang, and G. Yin, "Broken ring solitons in Bessel optical lattices," Opt. Lett. 33, 2989–2991 (2008).
- 44. H. Sakaguchi and B. A. Malomed, "Solitons in combined linear and nonlinear lattice potentials," Phys. Rev. A 81, 013624 (2010).
- 45. N. G. Vakhitov and A. A. Kolokolov, "Stationary solutions of the wave equation in the medium with nonlinearity saturation," Radiophys. Quant. El+ 16, 783–789 (1973).
- L. Bergé, "Wave collapse in physics: principles and applications to light and plasma waves," Phys. Rep. 303, 259–370 (1998).
- 47. Y. V. Kartashov, V. A. Vysloukh, and L. Torner, "Rotating surface solitons," Opt. Lett. 32, 2948–2950 (2007).